HiSST: 3rd International Conference on
High-Speed Vehicle Science Technology
14 -19 April 2024, Busan, Korea

Nozzle Flow Characterization of the SNU Hypersonic Shock Tunnel

Jinyoung Kim[1], Jinhwi Kim[2], Jungmu Hur[3], Bok Jik Lee[4], In Seuck Jeung[5]

Abstract

This paper presents the operational capabilities and the characteristics of the nozzle flow of the Seoul National University Hypersonic Shock Tunnel (SHyST), a recently added impulse facility designed to produce high enthalpy flows reaching up to 5 MJ/kg through hypersonic contoured nozzles. Within this investigation, emphasis is placed on the design and utilization of a pitot rake, serving as an essential instrument for quantifying pitot pressure and Mach number distributions throughout the test section. The experimental results confirm the presence of axis-symmetric behavior and spatial-temporal uniformity of the freestream Mach number at the nozzle outlet and along the test section. Additionally, the study demonstrates an excellent agreement with the predictions of numerical simulation. Mach number validation is further supported by the measurement of shock standoff distance through schlieren visualization.

Keywords: *Hypersonic Flow Experiments, Hypersonic Shock Tunnel, Reflected Shock tunnel, Flow Characterization*

Nomenclature

Latin

K – Density ratio across the shock wave

M – Mach number

P – Pressure

R_0 – Radius of the hemisphere

r – Radius from center of the nozzle

x – Axial distance

Greek

γ – Specific heat ratio

δ – Shock standoff distance

ρ – Density

Subscripts

s – Stagnation point

t – Total

1 – Ahead of the shock wave

2 – Behind the shock wave

1. Introduction

Advancements in aerospace technologies, like scramjet engines and re-entry capsules, emphasize the importance of understanding hypersonic flow dynamics. Hypersonic missions, which operate at extreme speeds, create high-temperature and non-equilibrium conditions in the flow field [1]. Impulsive facilities, such as reflected shock tunnels, replicate realistic hypersonic flight conditions by reaching

[1] *Department of Aerospace Engineering, Seoul National University, 1, Gwanak-ro, Gwanak-gu, Seoul, 08826, Republic of Korea, kimted@snu.ac.kr*
[2] *Department of Aerospace Engineering, Seoul National University, 1, Gwanak-ro, Gwanak-gu, Seoul, 08826, Republic of Korea, harrykim0814@snu.ac.kr*
[3] *Department of Aerospace Engineering, Seoul National University, 1, Gwanak-ro, Gwanak-gu, Seoul, 08826, Republic of Korea, gjwjdan135@snu.ac.kr*
[4] *Department of Aerospace Engineering, Seoul National University, 1, Gwanak-ro, Gwanak-gu, Seoul, 08826, Republic of Korea, b.lee@snu.ac.kr, Corresponding author*
[5] *Department of Aerospace Engineering, Seoul National University, 1, Gwanak-ro, Gwanak-gu, Seoul, 08826, Republic of Korea, enjis@snu.ac.kr*

high temperatures [2]. Despite their short testing durations, typically lasting milliseconds, these facilities offer sufficient time to analyze thermochemical and non-equilibrium effects at hypersonic speeds [3].

Recent developments in hypersonic testing infrastructure have been significant. Oxford University, for instance, introduced the T6 Stalker Tunnel, allowing ground simulation of various mission trajectories with total enthalpies ranging from 2.7 to 115.0 MJ/kg [4]. Similarly, Sandia National Laboratory unveiled a free-piston shock tunnel capable of achieving a total enthalpy of 4.6 MJ/kg within a 1ms test duration [5]. Additionally, the University of Queensland upgraded its reflected shock tunnel, X3R, enabling testing at Mach 7 with a diameter of 600mm and a test duration of 12.5ms [6]. These facilities not only support experimental studies but also improve numerical simulations, as demonstrated by Park et al.'s validation of numerical simulations for hypersonic inlets using data from seven distinct experimental cases [7].

The Seoul National University Hypersonic Shock Tunnel (SHyST), a recent addition to the institution's hypersonic research facilities, has a total length of 15 m and features a Mach 6.8 contoured nozzle. The primary objective of this paper is to present the current progress of commissioning SHyST, including initial measurements of flow characteristics within the test section. Section 2 provides an overview of SHyST's mechanical and operational design, while Section 3 describes the nozzle flow characterization methods, with a particular focus on pitot rake design and the utilization of the schlieren method for measuring shock standoff distance. Finally, Section 4 presents initial commissioning data results obtained from the described methods, along with a comparison with numerical simulation.

2. Facility Overview

As shown in Fig. 1, the SHySST consists of a driver tube and a driven tube, each with an inner diameter of 100 mm and lengths of 3 m and 8.2 m, respectively. The driver tube is rated for a maximum operating pressure of 30 MPa and can be filled with Nitrogen, Helium, or their combinations. It is connected to two high-pressure tanks containing each gas, enabling rapid filling within 2 minutes, and creating gas mixture according to Dalton's Law of Partial Pressures. The driven tube is typically filled with dry air or Nitrogen gas, with adjustable pressure.

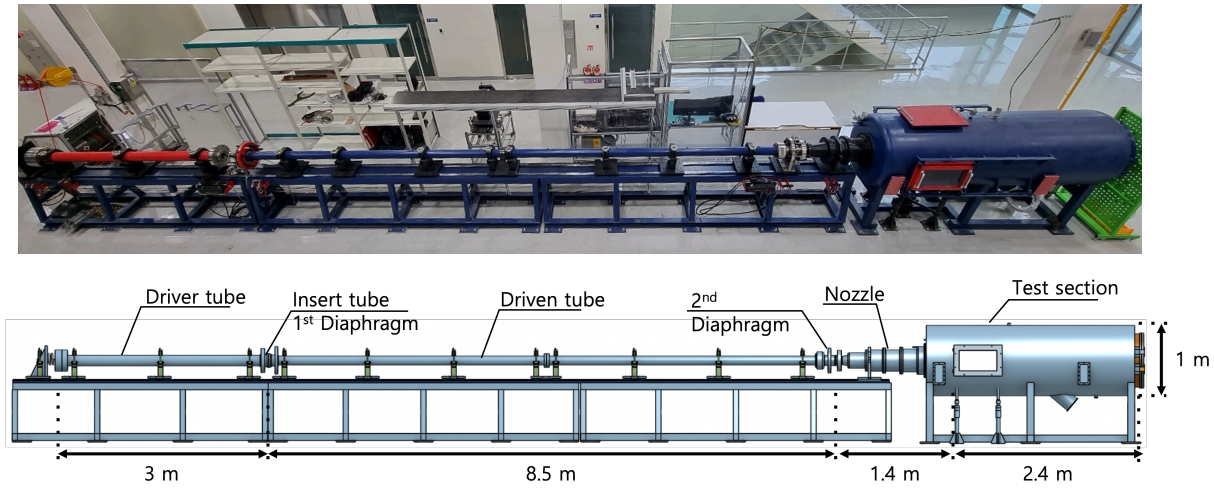

Fig 1. Photograph and Schematic of SHySST

The primary diaphragm is made of either a layer of 300 μm thick mylar films or a 5~6 mm thick Al1050 sheet, selected based on desired reservoir conditions. Aluminum diaphragms feature optimized +shaped grooves to ensure fully opened petal-shaped rupture for improved flow quality [8]. A secondary diaphragm, utilizing a 100 μm thick mylar film, is positioned within a removable throat insert. Hydraulic systems are used to secure diaphragms between tubes, preventing from gas leakage and diaphragm slippage. The facility currently operates with a Mach 6.8 converging-diverging nozzle, featuring a 0.34 m exit diameter and length of 1.4 m. Additionally, Mach 5 and Mach 6 contoured nozzles are currently in the process of being made. The test section has diameter of 1 m and length of

2.4 m, with depressurization capabilities down to 50 Pa. It comprises three windows—two on the sides and one above—each equipped with 15 mm thick quartz glass for optical measurements.

In the instrumental setup, a strain gauge pressure sensor (Sensys PMH series) is located at each tube to measure p1 and p4, as depicted in Fig. 2 (a). Additionally, three high-speed piezoelectric pressure transducers (PCB113b22) are positioned at distances of 18 mm, 518 mm, and 1518 mm upstream of the nozzle throat within the driven tube. These transducers serve to measure both shock speed and reservoir pressure p5 with higher frequency and faster response time. All sensors are recessed mounted to avoid contact with diaphragm debris. Data acquisition is facilitated by a signal conditioner (PCB483C05) connected to sensors, with data collected using a National Instruments PCIe 6376 (3.4 MHz bandwidth). Reservoir pressure, temperature, and total enthalpy within the nozzle under specific conditions are computed using a 1D thermochemical equilibrium solver, ESTCN [9]. Using three different nozzles, SHyST can analytically achieve total enthalpy up to 5 MJ/kg and Unit Reynold number up to 10^8 /m, as shown in Fig. 2 (b).

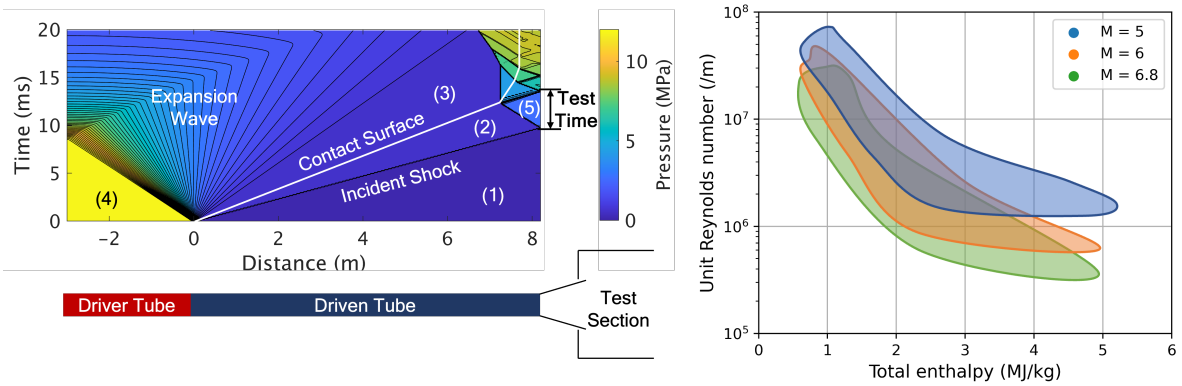

(a) (b)

Fig 2. (a) X-t diagrams of SHyST, (b) Performance envelope of SHyST with three different nozzle

The wave process within the shock tube region is depicted in Fig. 2 (a). The duration of the test time depends on achieving a steady condition in the reservoir, which is constrained by three mechanisms [10]. Primarily, there is the interaction between the reflected shock and the contact surface, leading to an additional expansion fan or shock. A stationary contact surface can be achieved by establishing a "tailored condition," through fine-tuning the gas composition and pressure in both the driver and driven tubes [11]. Second is the drainage rate of the reservoir gas and contact surface into the nozzle, which is primarily influenced by the diameter of the shock tube and the nozzle throat. Third is the arrival of the reflected expansion wave originating from the driver tube; delaying this reflection can extend the test duration. Additionally, the startup time of the nozzle, typically around 1 ms, should also be taken into account. Based on the experimental archive in SHyST, the test time ranges from 1~8 ms, depending on the gas setup condition in the shock tube.

3. Flow Characterization Method

3.1. Pitot Rake

The Pitot rake serves the purpose of evaluating the uniformity and axis-symmetry of pressure and Mach number along the test section. It comprises 12 high-speed pressure transducers (PCB 113B27) located at 30 mm intervals in a vertical non-symmetric configuration, as shown in Fig. 3 (b). Once axis-symmetry of the nozzle flow is confirmed, the spacing between the probes in the pitot rake is 15 mm, thus enhancing its spatial resolution. Each transducer is encased in a stainless-steel probe and protected by an internal porous shield. These shields act as safeguards for the sensors, shielding them from damage caused by diaphragm fragments.

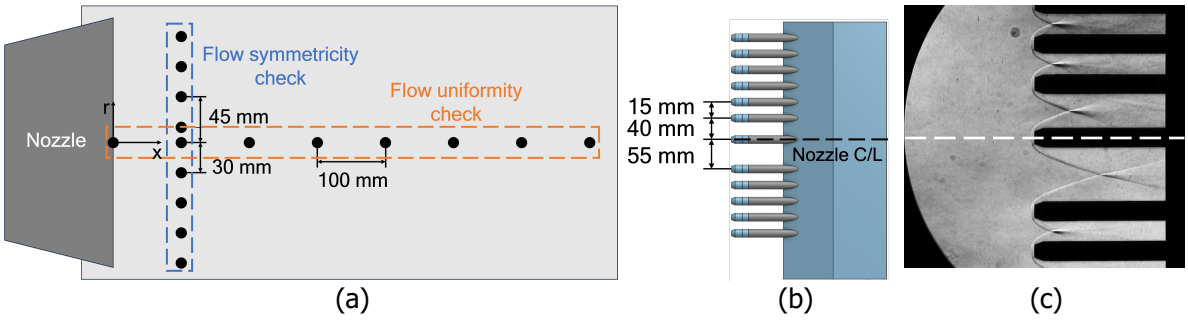

Fig 3. (a) Top view of the pitot rake flow measurement location, (b) Side view schematic and (c) schlieren photography of pitot rake

As illustrated in Fig. 3 (a), the pitot rake was placed at 100 mm from nozzle exit and measured the pitot pressure at 9 different uneven radial location to analyze the axis-symmetricity of the nozzle flow. For the uniformity analysis, the pitot rake was positioned at the center of the nozzle, and the axial distance (x) was varied by 100mm. A total of 17 experiments with different pitot rake location were conducted, maintaining consistent test flow conditions across all experiments. The average flow conditions are detailed in Table. 1, while Fig. 4 shows the reservoir pressure for all tests, demonstrating their close similarity.

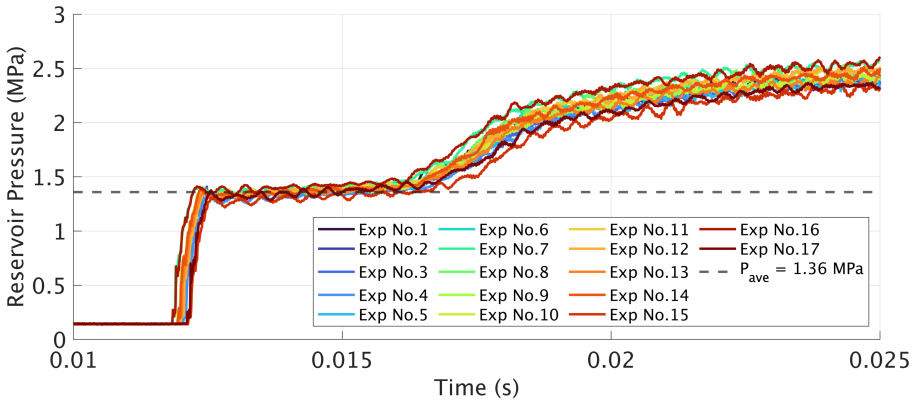

Fig 4. Reservoir pressure history of all pitot rake experiments

Table 1. Mean flow conditions for pitot rake experiment.

Driver gas	Driven gas	Reservoir pressure	Reservoir temperature	Total enthalpy	Reynolds number
Nitrogen	Dry air	1.36 Mpa	698.64 K	0.71 MJ/kg	0.49 x 10^7 /m

The pitot pressure data, sampled at the rate of 100 kHz, were converted into Mach numbers utilizing the Rayleigh pitot tube relation depicted in Eq. 1.

$$\frac{p_{t2}}{p_1} = \left[\frac{(\gamma+1)^2 M_1^2}{4\gamma M_1^2 - 2(\gamma-1)}\right]^{\gamma/(\gamma-1)} \frac{1-\gamma+2\gamma M_1^2}{\gamma+1} \quad (1)$$

In the above equation, P_{t2} is the pitot pressure, M_1 is the freestream Mach number and γ denotes the specific heat ratio obtained from Chemical Equilibrium with Applications (CEA), approximately 1.41. Static pressure P_1 was obtained through numerical simulation, OpenFOAM, using the reservoir and test chamber conditions. This approach was chosen due to its ability to provide a more accurate approximation compared to static pressure obtained from isentropic relations, particularly in the boundary layer region. Reynolds-Averaged Navier-Stokes (RANS) Simulation with k-ω SST turbulence model was applied. The HLLC scheme was utilized for the convective flux term, while a 3rd stage Runge-Kutta time integration scheme was implemented. Computational domain included the reservoir,

nozzle, and test section, having around 30,000 cells and y^+ of 30~60 at wall, applying a no-slip condition and wall function, as depicted in Fig. 5.

To validate the CFD result, a comparison was first done between the pitot pressure obtained from CFD freestream data and experimental measurements. Schlieren photography was also taken to confirm the presence of a normal shock in front of the pitot probes, ensuring the appropriate utilization of the Rayleigh pitot tube relation, as shown in Fig. 3 (c).

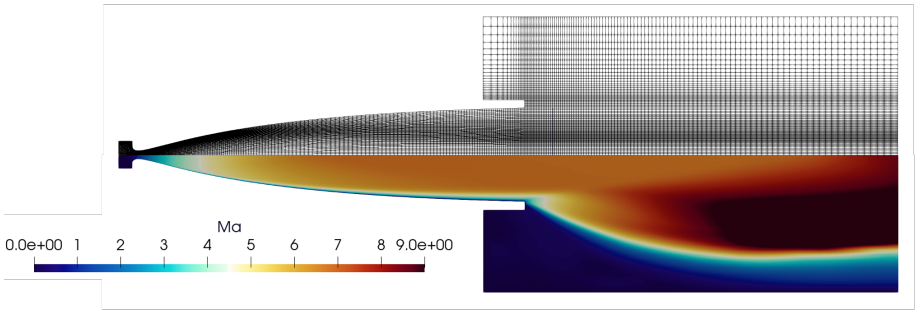

Fig 5. Computational grid for nozzle flow simulation

3.2. Shock Standoff Distance around Hemisphere

A conventional Z-type schlieren method was employed to visualize the flow structure and determine the freestream Mach number by measuring the shock standoff distance with a 55 mm radius hemisphere model. In the schlieren setup, continuous LED lighting was used as the light source, while a Phantom V710 camera captured images with an exposure time of 130 μs and a frame rate of 7,500 fps. The schlieren photography was taken under identical condition as outlined in Table. 1.

To establish the relationship between shock standoff distance and Mach number, two empirical relations were compared with the obtained standoff distance: (1) the relations provided by Serbin [12], and (2) the relations provided by Van Dyke and Lobb [13, 14]. Serbin's relation indicates that the shock standoff distance varies according to the density ratio across the shock wave,

$$\frac{\delta}{R_0} = \frac{2}{3}(K-1)^{-1} \tag{2}$$

In the above equation, δ is the shock standoff distance along the stagnation line, and $R_0 = 55\,mm$ denotes the radius of the hemisphere. The density ratio across the shock wave is denoted as $K = \rho_s/\rho_1$, and it can be written in terms of normal shock wave relation,

$$K = \frac{\rho_s}{\rho_1} = \left[\frac{M_1^2(\gamma+1)^2}{4\gamma M_1^2 - 2(\gamma-1)}\right]^{\frac{1}{\gamma-1}} \frac{(\gamma+1)M_1^2}{2+(\gamma-1)M_1^2} \tag{3}$$

Utilizing the provided relationship, the Mach number was calculated using the measured value of $\frac{\delta}{R_0}$ from the schlieren visualization. On the other hand, the Lobb's approximation is derived from the experiments and numerical analysis of Van Dyke for non-reactive gas, which exhibits a similar relation but with a different correlation factor,

$$\frac{\delta}{R_0} = 0.82\frac{1}{\mathrm{K}} \tag{4}$$

The estimated Mach number from these two methods were compared with results from the pitot rake experiments.

4. Results and Discussion

4.1. Pitot Rake

Fig. 6 (a) illustrates the nozzle startup time, approximately 1.5 ms. The time-position contour plot depicted in Fig. 6 (b) indicates that the flow at the exit of the nozzle (x = 0 mm) maintains temporal uniformity for around 3 ms, thereby determining the effective test time. Subsequently, the pressure increases due to the over-tailored condition at the reservoir.

Both the pitot and reservoir pressure data exhibit some oscillation and uncertainty, potentially stemming from their mounting type, recessed mount, where the cavity in front of the transducer can induce acoustic resonance [15]. This resonance may also contribute to delaying the rise time. Eghblom et al. [16] suggested that for cases involving small cavities, the acoustic resonance is attributed to freestream noise. Therefore, Freestream noise was calculated to determine the level of noise present in the SHyST freestream, as shown in Table 2, using a simple equation: Noise Level (%) = $\frac{P'_{t2,rms}}{P_{t2,mean}}$. Data points P1 – P7 represent the uniform flow region, while P8 -P10 are in the boundary layer region, where the flow is non-uniform. When accounting for the uniform region only, the mean noise level is calculated to be 4.08%. Compared to other hypersonic facilities that are surveyed in [17], the SHyST freestream is deemed "noisy," a characteristic sufficient to cause acoustic resonance in the cavity near the pressure sensors. This may also induce laminar-turbulent transition earlier than observed in actual flight experiments in hypersonic regime [18].

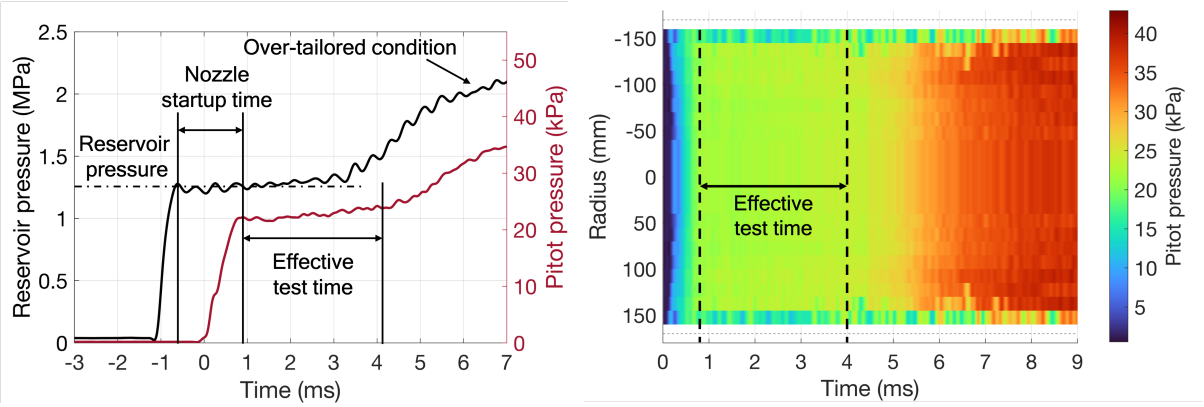

(a) (b)

Fig 6. (a) Reservoir & pitot pressure at nozzle centre, (b) Pitot pressure contour plot at nozzle exit

Table 2. Freestream noise level at x = 100 mm

Parameters	P1	P2	P3	P4	P5	P6	P7	P8	P9	P10
Radial Location (mm)	0	40	55	70	85	100	115	130	145	160
Noise Level (%)	5.00	3.53	3.18	4.01	6.08	3.60	3.15	18.70	16.58	50.87

Fig. 7 (a) shows the pitot pressure data in vertical and horizontal directions at x = 100 mm, with error bars representing the standard deviation of variation during the test time. The experimental results demonstrate axis-symmetrical behavior and exhibit strong agreement with the pitot pressure obtained from the CFD result in both directions. This consistency suggests that the CFD solution effectively approximates the actual nozzle flow field. Consequently, the static pressure P_1 obtained from CFD simulation is utilized to convert the pitot pressure data into Mach numbers. As shown in Fig. 7 (b), a total 119 experimental data points at the x = 100 mm plane were converted into Mach number, and they also show good agreement with the CFD results.

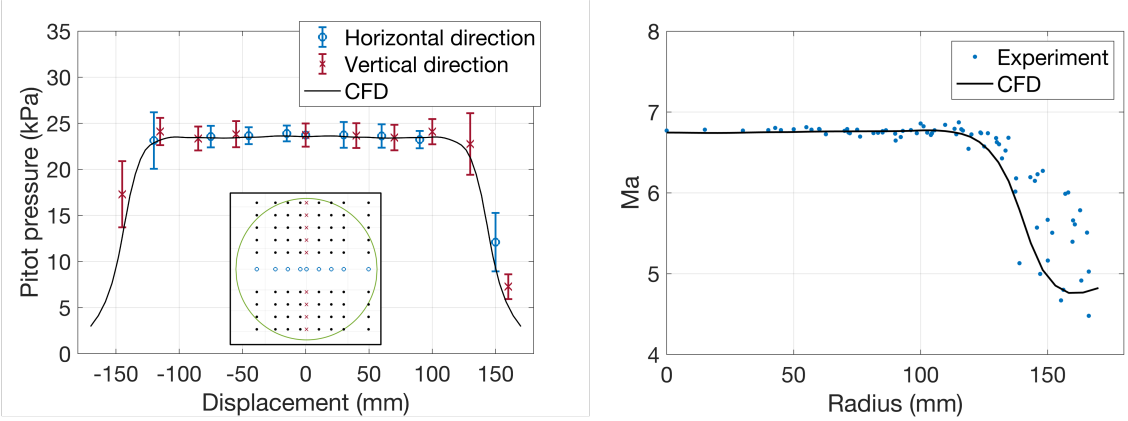

(a) (b)

Fig 7. (a) Horizontal and vertical pitot pressure distribution and (b) Mach number distribution at axial distance x = 100 mm

The Mach number distribution along the test section, as depicted in Fig. 8, reveals a uniform flow near the nozzle, spanning approximately 220 mm in diameter, equivalent to 65% of the nozzle exit diameter. However, as the flow progresses away from the nozzle, the uniformity diminishes due to expansion originating from the nozzle tip. In the region between 100 and 500 mm, a slight disparity is observed at the end between the numerical and experimental results. This discrepancy arises from the non-axisymmetric geometry of the test chamber, which includes observation windows and a test model installation bed in this area. Nonetheless, this disparity does not significantly affect the determination of the uniform flow region.

This result delineates the uniform Mach region at 6.76, highlighted by the blue-colored region in Fig. 8. It's important to note that the Mach number varies based on the reservoir enthalpy. Research by Chan et al. [19] suggests that altering reservoir temperature has a more pronounced effect on Mach number than reservoir pressure due to the higher ratio of specific heat at lower reservoir temperatures. According to the nozzle area ratio–Mach number relations for ideal gas compressible flows, a higher ratio of specific heats with the given nozzle area ratio results in a higher Mach number. Conversely, varying reservoir pressure has a significantly lesser effect on flow uniformity at the nozzle exit compared to altering reservoir temperature.

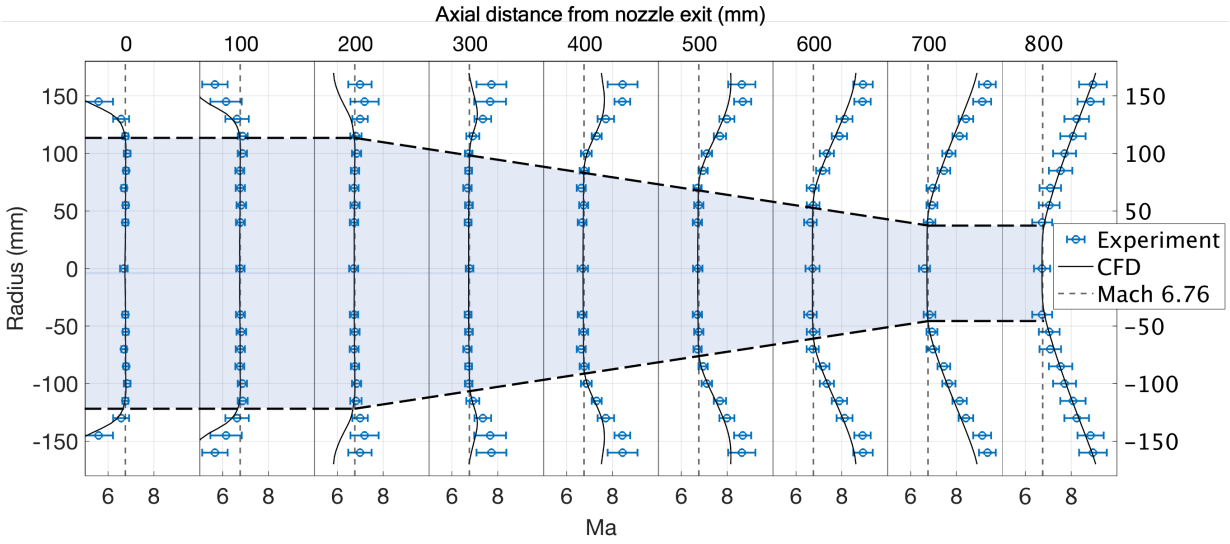

Fig 8. Mach number distribution along the test section

To investigate the impact of variations in reservoir conditions on flow quality and the uniform flow region, two additional experiments were conducted under different reservoir conditions, as outlined in Table 3. The reservoir temperature was increased by up to 2.3 times, while the pressure was increased by up to 6.8 times, resulting in relatively higher enthalpy compared to the original experiments (case

1). Measurements for these experiments were also taken at x = 100 mm, and numerical simulations were performed accordingly.

As depicted in Fig. 9, the maximum difference in pitot-to-reservoir pressure among the three cases was 0.001 within the core flow region (r = 110 mm). When compared with the experimental data, this difference falls within the uncertainties of all experimental data within the core flow region. Note that experimental data for case 2 at r = 70 mm are deemed erroneous, likely due to the transducer being struck and obstructed by diaphragm debris. Despite significant variations in reservoir conditions, there appear to be no substantial differences in pitot pressure distribution. Although the Mach number may vary, the pitot-to-reservoir pressure ratio remains insensitive to the reservoir condition, suggesting that the uniform region of the nozzle freestream flow within the test section remains consistent in size despite changes in test conditions.

Table 3. Three different reservoir conditions for flow quality analysis

Case	Reservoir pressure (Mpa)	Reservoir temperature (K)	Total enthalpy (MJ/kg)
1 (original)	1.36	698.64	0.71
2	9.18	1498.27	1.65
3	7.42	1604.34	1.78

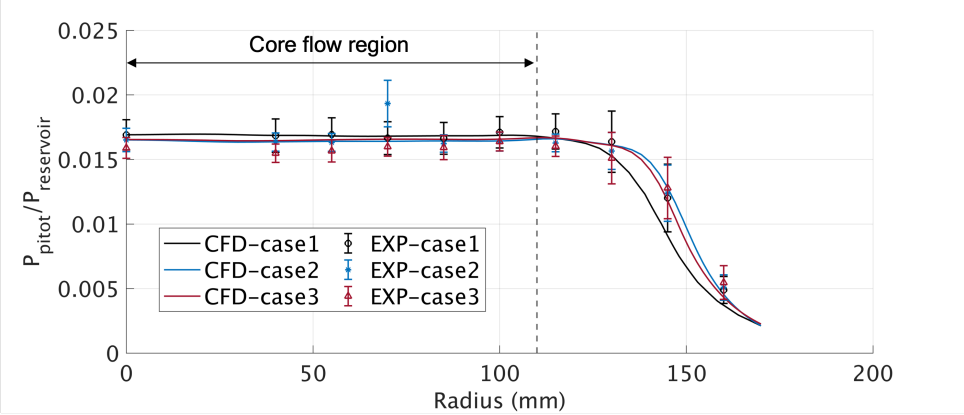

Fig 9. Pitot-to-reservoir pressure distribution at x = 100mm

4.2. Shock Standoff Distance around Hemisphere

As presented in Fig. 10 (a), the shock standoff distance was determined through schlieren photography using a basic pixel correlation technique. The resulting δ/R_0 obtained in this experiment was 0.141 ± 0.001, which was subsequently converted into a Mach number range using Eq. (2) - (4). Fig. 10 (b) shows that Serbin's method yielded a calculated Mach number of 6.68 ± 0.21, while Lobb's method resulted in 7.32 ± 0.35. When comparing these Mach numbers with those obtained from the pitot rake experiment (6.76), Serbin's method demonstrated reasonable agreement, with a maximum difference of approximately 5%. This finding is consistent with experiments conducted by Park et al. [20] and Seanz et al. [21] at different facilities.

It's noteworthy that both methodologies assume perfect gas behavior. However, freestream flow through the nozzle with high enthalpy exhibits a higher degree of complexity, characterized by thermo-chemical non-equilibrium [22]. This complexity can result in discrepancies in shock standoff distance between ideal gas and real gas conditions. Extensive research efforts have been directed towards elucidating this phenomenon [23]. Importantly, our experiments were conducted under very low enthalpy conditions, where real gas effects are minimized, thereby exhibiting closer alignment with the Serbin's semi-theoretical model.

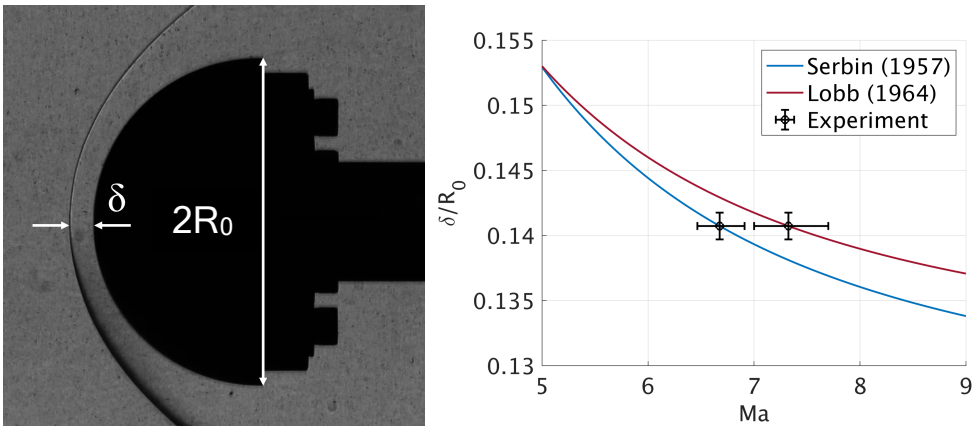

(a) (b)

Fig 10. (a) Schlieren visualization around a hemisphere, (b) Mach number comparison

5. Conclusion

This study has investigated the nozzle flow characteristics of the Seoul National University Hypersonic Shock Tunnel (SHyST). The stagnation properties of nozzle supply were computed by 1D thermochemical equilibrium solver using experimental data obtained from the current facility, demonstrating its capability to generate total enthalpy up to 5 MJ/kg. The development and implementation of a high spatial-resolution pitot rake have facilitated the validation of computational fluid dynamics (CFD) results, confirming the axis-symmetry and uniformity of the nozzle flow within the test section, with an estimation of a freestream Mach number of approximately 6.8. Additionally, noise level analysis has been conducted to evaluate pressure data oscillations and uncertainty, which were than compared with other facilities. Examinations of freestream flow under different reservoir conditions revealed that the uniform flow region remains unaffected by such variations. Furthermore, the measurements of shock standoff distance through schlieren visualization provided reaffirmation of the Mach number. Moving forward, future efforts will focus on characterizing flow dynamics around hypersonic vehicle models such as Earth and Mars entry vehicles for space exploration, including the investigation of thermo-chemical nonequilibrium and boundary layer transition phenomena in high-enthalpy environments.

6. Acknowledgements

This research was supported by the Challengeable Future Defense Technology Research and Development Program through the Agency For Defense Development (ADD) funded by the Defense Acquisition Program Administration (DAPA) in 2023(No.915067201). Jinyoung Kim, Jinhwi Kim, and Jungmu Hur contributed equally to this work.

References

1. Marren, D., Lu, F. eds: Advanced Hypersonic Test Facilities. American Institute of Aeronautics and Astronautics, Reston ,VA (2002)
2. Lee, B.J., Lee, H.J., Kim, S.H., Jeung, I.S.: Design/Construction and Performance Test of Hypersonic Shock Tunnel Part Ⅰ: Design Method of Hypersonic Shock Tunnel. Journal of the Korean Society for Aeronautical & Space Sciences. 36, 321－327 (2008). https://doi.org/10.5139/JKSAS.2008.36.4.321
3. Lu, F., Wilson, D.: Survey of short duration, hypersonic and hypervelocity facilities. In: 25th Plasmadynamics and Lasers Conference. American Institute of Aeronautics and Astronautics, Colorado Springs,CO,U.S.A. (1994)
4. Collen, P., Doherty, L.J., Subiah, S.D., Sopek, T., Jahn, I., Gildfind, D., Penty Geraets, R., Gollan, R., Hambidge, C., Morgan, R., McGilvray, M.: Development and

commissioning of the T6 Stalker Tunnel. Exp Fluids. 62, 225 (2021). https://doi.org/10.1007/s00348-021-03298-1

5. Lynch, K.P., Grasser, T., Farias, P., Daniel, K., Spillers, R., Downing, C.R., Wagner, J.L.: Design and Characterization of the Sandia Free-Piston Reflected Shock Tunnel. In: AIAA SCITECH 2022 Forum. American Institute of Aeronautics and Astronautics, San Diego, CA & Virtual (2022)
6. Stennett, S.J., Gildfind, D., Jacobs, P., Morgan, R., James, C., Toniato, P.: The X3R Free-Piston Reflected Shock Tunnel: Australia's New Large-Scale, Long-Duration Hypersonic Testing Capability. In: 23rd AIAA International Space Planes and Hypersonic Systems and Technologies Conference. American Institute of Aeronautics and Astronautics, Montreal, Quebec, Canada (2020)
7. Park, Y., Nam, J., Kim, Y., Jun, D., Lee, B.J., Lee, Y.J.: Validation of numerical simulations for investigating flow control in hypersonic inlets. Aerospace Science and Technology. 140, 108452 (2023). https://doi.org/10.1016/j.ast.2023.108452
8. Anbuselvan, K.K.N., Reddy, K.P.J.: Improvement in the Flow Quality of Hypersonic Shock Tunnel. AIAA Journal. 55, 3603–3610 (2017). https://doi.org/10.2514/1.J055523
9. Jacobs, P.A., Gollan, R.J., Potter, D. F., Zander, F., Gildfind, D.E., Blyton, P., Chan, W.Y.K., Doherty, L.: Estimation of high-enthalpy flow conditions for simple shock and expansion processes using the ESTCj program and library, St Lucia, QLD, Australia (2014)
10. Campbell, M.F., Parise, T., Tulgestke, A.M., Spearrin, R.M., Davidson, D.F., Hanson, R.K.: Strategies for obtaining long constant-pressure test times in shock tubes. Shock Waves. 25, 651–665 (2015). https://doi.org/10.1007/s00193-015-0596-x
11. Wittliff, C.E., Wilson, M.R., Hertzberg, A.: The Tailored-Interface Hypersonic Shock Tunnel. Journal of the Aerospace Sciences. 26, 219–228 (1959). https://doi.org/10.2514/8.8016
12. Serbin, H.: Supersonic Flow Around Blunt Bodies. Journal of the Aerospace Sciences. 25, 58–59 (1958). https://doi.org/10.2514/8.7487
13. Van Dyke, M.D.: The Supersonic Blunt-Body Problem - Review and Extension. Journal of the Aerospace Sciences. 25, 485–496 (1958). https://doi.org/10.2514/8.7744
14. Lobb, R.K.: Chapter 26 - Experimental Measurement of Shock Detachment Distance on Spheres Fired in Air at Hypervelocities. In: Nelson, W.C. (ed.) AGARDograph. pp. 519–527. Elsevier (1964)
15. McGilvray, M., Jacobs, P.A., Morgan, R.G., Gollan, R.J., Jacobs, C.M.: Helmholtz Resonance of Pitot Pressure Measurements in Impulsive Hypersonic Test Facilities. AIAA Journal. 47, 2430–2439 (2009). https://doi.org/10.2514/1.42543
16. Engblom, W.A., Goldstein, D.B., Ladoon, D., Schneider, S.P.: Fluid Dynamics of Hypersonic Forward-Facing Cavity Flow. Journal of Spacecraft and Rockets. 34, 437–444 (1997). https://doi.org/10.2514/2.3255
17. Alba, C., Casper, K., Beresh, S., Schneider, S.: Comparison of Experimentally Measured and Computed Second-Mode Disturbances in Hypersonic Boundary-Layers. In: 48th AIAA Aerospace Sciences Meeting Including the New Horizons Forum and Aerospace Exposition. American Institute of Aeronautics and Astronautics, Orlando, Florida (2010)
18. Schneider, S.P.: Effects of High-Speed Tunnel Noise on Laminar-Turbulent Transition. Journal of Spacecraft and Rockets. 38, 323–333 (2001). https://doi.org/10.2514/2.3705
19. Chan, W.Y.K., Jacobs, P.A., Smart, M.K., Grieve, S., Craddock, C.S., Doherty, L.J.: Aerodynamic Design of Nozzles with Uniform Outflow for Hypervelocity Ground-Test

Facilities. Journal of Propulsion and Power. 34, 1467–1478 (2018). https://doi.org/10.2514/1.B36938

20. Park, S.H., Park, G.: Separation Process of Spheres in Hypersonic Flows. In: 2018 AIAA Atmospheric Flight Mechanics Conference. American Institute of Aeronautics and Astronautics, Kissimmee, Florida (2018)
21. Saenz, L., Vergeer, L., Frankel, J., Shu, F.: Characterization of the Mach 5 Shock Tunnel at New Mexico State University. In: AIAA AVIATION 2023 Forum. American Institute of Aeronautics and Astronautics, San Diego, CA and Online (2023)
22. Kim, I., Lee, S., Park, G., Lee, J.K.: Overview of Flow Diagnosis in a Shock Tunnel. International Journal of Aeronautical and Space Sciences. 18, 425–435 (2017). https://doi.org/10.5139/IJASS.2017.18.3.425
23. Belouaggadia, N., Olivier, H., Brun, R.: Numerical and theoretical study of the shock stand-off distance in non-equilibrium flows. J. Fluid Mech. 607, 167–197 (2008). https://doi.org/10.1017/S0022112008001973